The Generation of Equatorial Transient Planetary Waves: Control Experiments with a GFDL General Circulation Model

Y. HAYASHI AND D. G. GOLDER

Geophysical Fluid Dynamics Laboratory, NOAA, Princeton University, Princeton, NJ 08540

(Manuscript received 1 May 1978, in final form 21 July 1978)

ABSTRACT

In order to study the generation of transient planetary waves in the tropics, the effects of topography, midlatitude disturbances and condensational heat are eliminated one by one from a GFDL general circulation model during the period June and July. The time development and three-dimensional propagation of waves are examined by a space-time spectral analysis using the maximum entropy method.

It is found that the characteristic scale and period of Kelvin and mixed Rossby-gravity waves do not depend on land-sea contrast or the zonal variation of sea surface temperature. Even if midlatitude disturbances are eliminated, both these waves appear in the stratosphere due to the effect of latent heat release in the troposphere. In contrast to Kelvin waves, however, mixed Rossby-gravity waves can be significantly intensified by westward moving midlatitude disturbances which are found to propagate intermittently toward the equator.

1. Introduction

There has been significant progress in observational and theoretical studies of equatorial planetary waves since the discovery of mixed Rossby-gravity waves by Yanai and Maruyama (1966) and Kelvin waves by Wallace and Kousky (1968) in the equatorial stratosphere. Both of these waves were demonstrated by Hayashi (1974) to be well simulated by a GFDL general circulation model and were also detected by Tsay (1974) in a NCAR general circulation model.

The observed mixed Rossby-gravity waves are associated with wavenumbers 3–5 and periods of 4–6 days and travel westward. Since they take the form of vortices centered over the equator, their zonal and meridional components attain their minimum and maximum over the equator, respectively. They tilt westward with height in the stratosphere and transport westerly momentum and energy upward. These waves are consistent with wavenumber-frequency relationships of equatorial normal modes studied by Matsuno (1966), Rosenthal (1965), Lindzen (1967) and Lindzen and Matsuno (1968). These waves may, in part, be responsible for the easterly acceleration of the quasi-biennial oscillations of the equatorial stratospheric zonal wind (Reed *et al.*, 1961), since the theoretical mixed Rossby-gravity waves accelerate the easterlies due to the net effect of induced meridional circulation and wave momentum transport (Hayashi, 1970; Lindzen, 1970; Andrews and McIntyre, 1976).

On the other hand, the observed Kelvin waves are associated with wavenumbers 1–2 and periods of 10–20 days, travel eastward and are characterized by the absence of a meridional wind component. Kelvin waves tilt eastward with height in the stratosphere and transport westerly momentum and energy upward. These waves have been shown to be responsible for the westerly acceleration of the quasi-biennial oscillation both observationally and theoretically.

There have been several theoretical studies to explain the generation and selection of these waves. The first approach was a theory of reasonance to midlatitude forcing by Mak (1969). He found that westward moving equatorial waves exhibit a large resonant response at a period of 4 days with wavenumber 4 and derive their energy from midlatitude disturbances whose meridional component was imposed at 30° latitude. His result is also consistent with wave propagation theories. According to Charney (1969), Dickinson (1968) and Bennett and Young (1971), waves moving westward relative to the basic wind can propagate into the tropics, provided the horizontal shear is not too strong (Gambo, 1971) and the vertical scale is not too short (Murakami, 1973; Chang, 1974). Lamb (1973) further showed that the amplitude of the laterally forced wave can be enhanced significantly by including a parameterized effect of latent heat release.

Subsequently, Hayashi (1976) reexamined Mak's theory by imposing the radiation condition at the top of the atmosphere. His result provided assurance that the reflecting upper boundary condition in a finite-difference model is not a serious defect for equatorial waves with small vertical group velocity since they are

significantly dissipated before reaching the top. He confirmed that even if wave energy is not reflected from above, a "nonsingular resonance" with a large finite amplitude occurs when the vertical scale of the wave coincides with that of the lateral forcing. However, he also noted that the horizontal structure of the resonant wave does not take the form of observed mixed Rossby-gravity waves. Moreover, the resonant wave is associated with a very sharp spectral peak in the meridional flux of energy at the lateral boundary, whereas this peak is not detected in a GFDL general circulation model. Quite recently, Itoh (1978) showed the resonant wave takes the form of observed mixed Rossby-gravity waves if the lateral boundary forcing is replaced by a body (thermal) forcing in midlatitudes. However, his theory predicts sharp resonant peaks in the parameterized tropical precipitation, whereas these peaks are not clearly detected in a GFDL general circulation model (Hayashi, 1974).

The second approach was an instability (CISK) theory by Hayashi (1970), extending the work of Yamasaki (1969) to equatorial waves. This theory assumes that convective heating is proportional to surface convergence due to large-scale waves. It was found that instability is possible for mixed Rossby-gravity waves and Kelvin waves with realistic three-dimensional structure. However, their preferred scale did not agree with that observed, although this difficulty can be avoided by assuming that cumulus heating becomes inefficient for high-frequency waves due to the constraint of moisture availability (Hayashi, 1971a; Kuo, 1975). Moreover, the CISK theories also predict sharp spectral peaks in the tropical rainfall which are not clearly detected in a general circulation model (Hayashi, 1974).

Further studies by Lindzen (1974) and Chang (1976a) indicate that the vertical scale of the most unstable waves is sensitive to the depth of the surface layer and the vertical profile of heating. Recently, Stark (1976) argued that instability is not possible for vertically propagating large-scale equatorial waves based on a linearized Arakawa parameterization scheme (Arakawa and Schubert, 1974) in which cumulus heating is related to the vertical velocity at all levels.

The third approach was to examine the response of the atmosphere to random thermal forcing in the presence of a vertical wind shear. Holton (1972) demonstrated that both eastward and westward moving waves were excited in the troposphere by a localized tropospheric heat source pulsating with an imposed periodicity, while either eastward moving Kelvin waves or westward moving mixed Rossby-gravity waves with observed wavenumber propagate into the stratosphere, depending on the vertical profile of wind. It was further pointed out by Holton (1973) that a 10–20 day spectral peak in tropospheric thermal forcing is not required to account for the observed spectral distribution of stratospheric Kelvin waves,

TABLE 1. The normalized pressure and approximate height of the levels used in the model.

Level	$\sigma = P/P_*$	Height (m)
1	0.015	28 469
2	0.035	22 789
3	0.058	19 545
4	0.098	16 219
5	0.166	12 877
7	0.259	10 019
7	0.374	7547
8	0.502	5434
9	0.635	3661
10	0.761	2240
11	0.870	1157
12	0.950	430
13	0.991	76

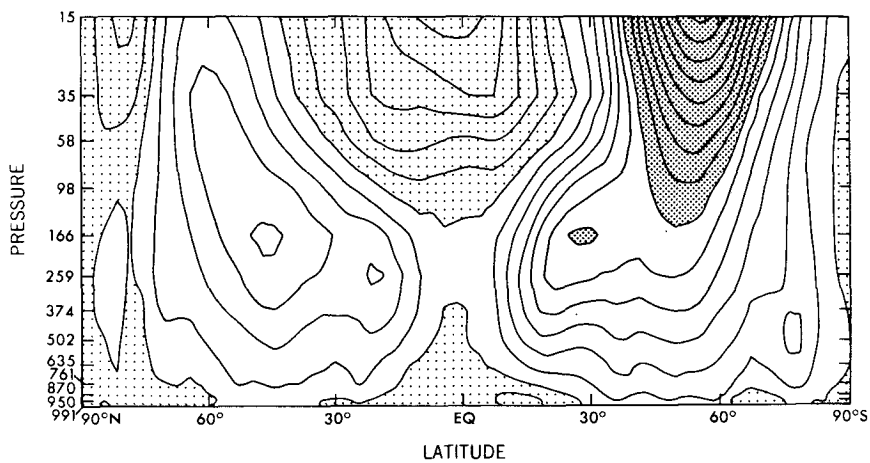

FIG. 1. Latitude-height distribution of the simulated zonal mean wind (m s^{-1}), for model day 1 June. Contour interval 5 m s^{-1}; light shade $\leqslant 0.0$, dark shade $\geqslant 30.0$.

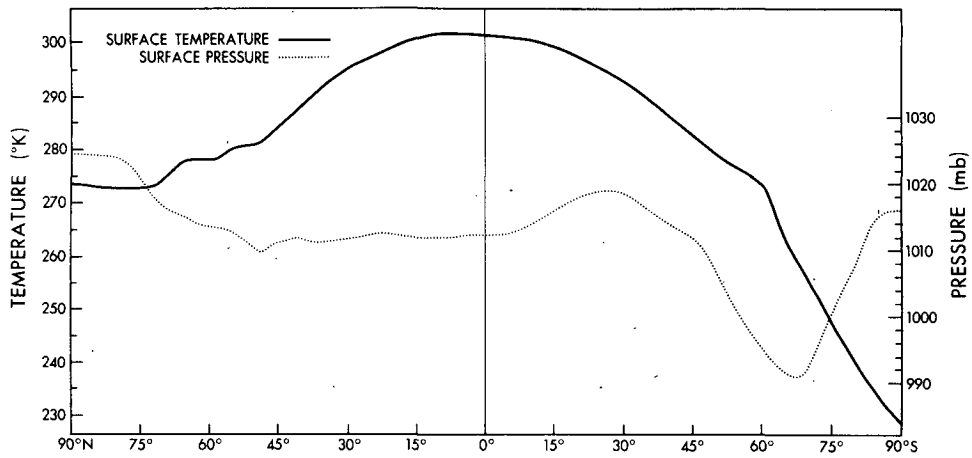

FIG. 2. Latitudinal distribution of longitudinally averaged sea surface temperature and surface pressure of the model in June.

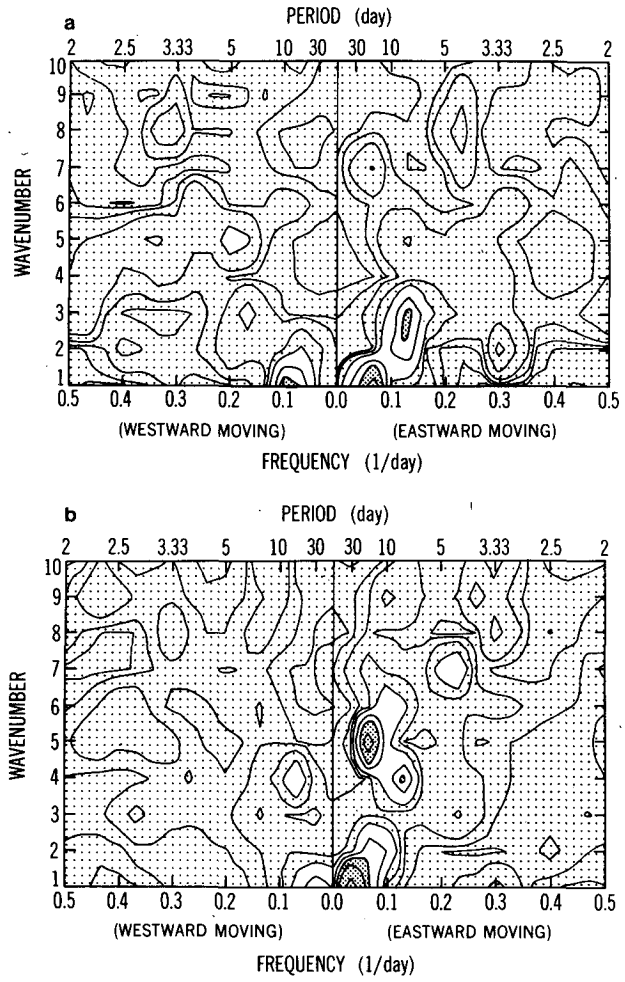

FIG. 3. Frequency-wavenumber diagram of the power spectrum of the zonal wind over the equator for the model period 12–26 July at level 35 mb (a) and 166 mb (b). Contour values 5.0, 10.0, 20.0, 30.0, 50.0 $m^2 s^{-2}$ day; light shade ≤ 5.0, dark shade ≥ 30.0.

since the atmosphere acts as a bandpass filter to select these waves. This point was confirmed by the spectral analysis of the GFDL general circulation model (Hayashi, 1974).

Subsequently, Hayashi (1976) and Chang (1976b) showed that such wavenumber-frequency selection for equatorial modes occurs even without vertical wind shear due to the "resonant" response to tropospheric heating under the radiation condition when the vertical scale of the wave coincides with that of the tropospheric heating. However, Hayashi noted that the vertical structure of the resonant wave is not realistic. This defect was confirmed by Itoh (1977) based on a model which is similar to Holton's (1972) model with a realistic meridional profile of heating and vertical wind shear. In reality such resonance may not occur if there is a strong mutual interaction between heating and the wave.

In view of the defects and controversies among these linear theories, we feel control experiments with a general circulation model will clarify to some extent the causes of the generation of equatorial planetary waves. The first point of interest is the topographical effect on the characteristic scale of these waves, although this effect is not crucial in the abovementioned theories. The second point is the effect of midlatitude disturbances which is essential in lateral forcing theories. The third point is the effect of condensational heat which is essential in both the CISK theories and thermal forcing theories. Our approach is to eliminate these effects one by one from the model in order to identify their role in the generation of equatorial waves.

2. Basic model

The basic model is essentially the same as the global model constructed by Manabe *et al.* (1974)

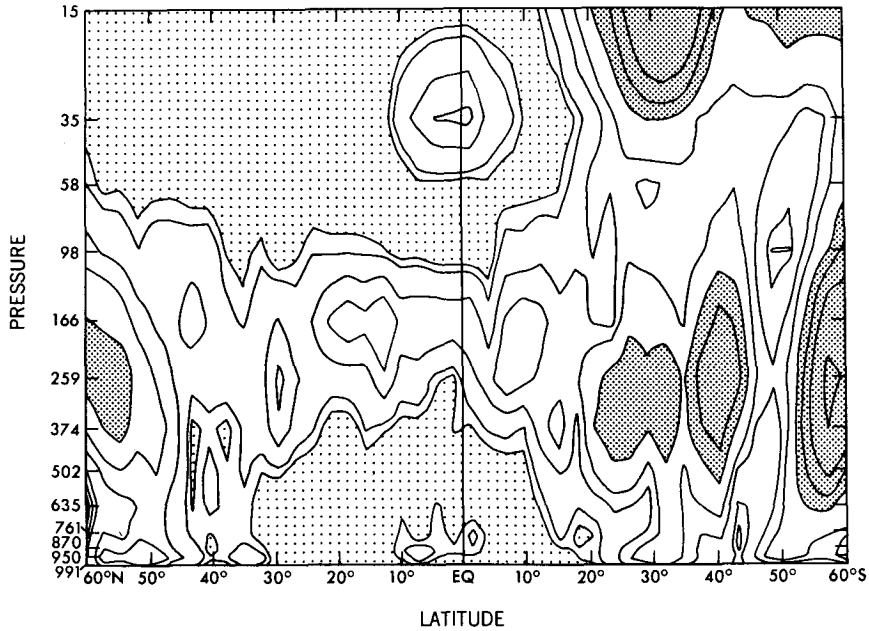

FIG. 4. Latitude-height distribution of the power spectrum of the zonal wind (wavenumber 1–2, period 10–15 days, eastward moving) during the model period 12–26 July. Contour values 0.7, 1.0, 2.0, 3.0, 5.0, 7.0, 10.0, 20.0 $m^2 s^{-2}$; light shade ≤ 0.7, dark shade ≥ 5.0.

with orography, moist convective adjustment and seasonal variation. The tropical general circulation as simulated by the model is described by Manabe *et al.* (1974). A detailed analysis of transient waves appearing in this model was made by Hayashi (1974). The present model differs in that it has a latitude-longitude grid (Holloway *et al.*, 1973; Manabe *et al.* 1975) with 64×128 grid points in the horizontal and 13 levels in the vertical (see Table 1 for the vertical spacing). The initial conditions for this model were interpolated from the 1 June data of an 11-layer general circulation model (Manabe *et al.*, 1974). The zonal mean wind as found in the latitude-height domain is shown in Fig. 1.

3. The topographical effect and wave development

The first experiment is to eliminate the topographical effects of land and sea. This experiment excludes not only stationary waves, but also standing wave oscillations, since there is no topographical effect to fix their nodes and antinodes. It will be of interest to examine whether stratospheric traveling waves appear in the absence of standing wave oscillations in the troposphere, which consist of both eastward and westward moving components appearing simultaneously. According to Hayashi (1974), the local amplitude of simulated equatorial waves exhibits significant longitudinal variations due to topographical effects. It is of interest to examine whether the characteristic scale and period of these waves are also significantly influenced by these effects.

The topographical effects were eliminated by replacing the model's surface points with ocean points having zonally uniform temperatures. These temperatures were taken from the zonal mean of the model's sea surface temperature (see Fig. 2) which is based on observation. On 2 June longitudinal perturbations of the predicted variables were set to zero and a small random perturbation was added to the temperature field. The numerical time integration was carried out for 60 days.

It is also of interest in this section to analyze how these waves develop from small random disturbances and propagate vertically and horizontally. For this purpose, a space-time spectral analysis (see Appendix A) was made employing the recent technique of the maximum entropy method which yields finer frequency resolutions for a shorter record than conventional methods. The power spectrum was computed for 10 overlapping time segments with a time interval of 15 days to examine the temporal development of wave amplitude.

a. The Kelvin wave

Fig. 3 shows a frequency-wavenumber diagram of the power spectrum of the zonal wind over the equator at the 35 mb (a) and 166 mb (b) levels. These figures represent the period 12–26 July during which stratospheric Kelvin waves appear most distinctly in this experiment. In the stratosphere (Fig. 3a) a spectral peak is found at wavenumber 1–2 and a period of

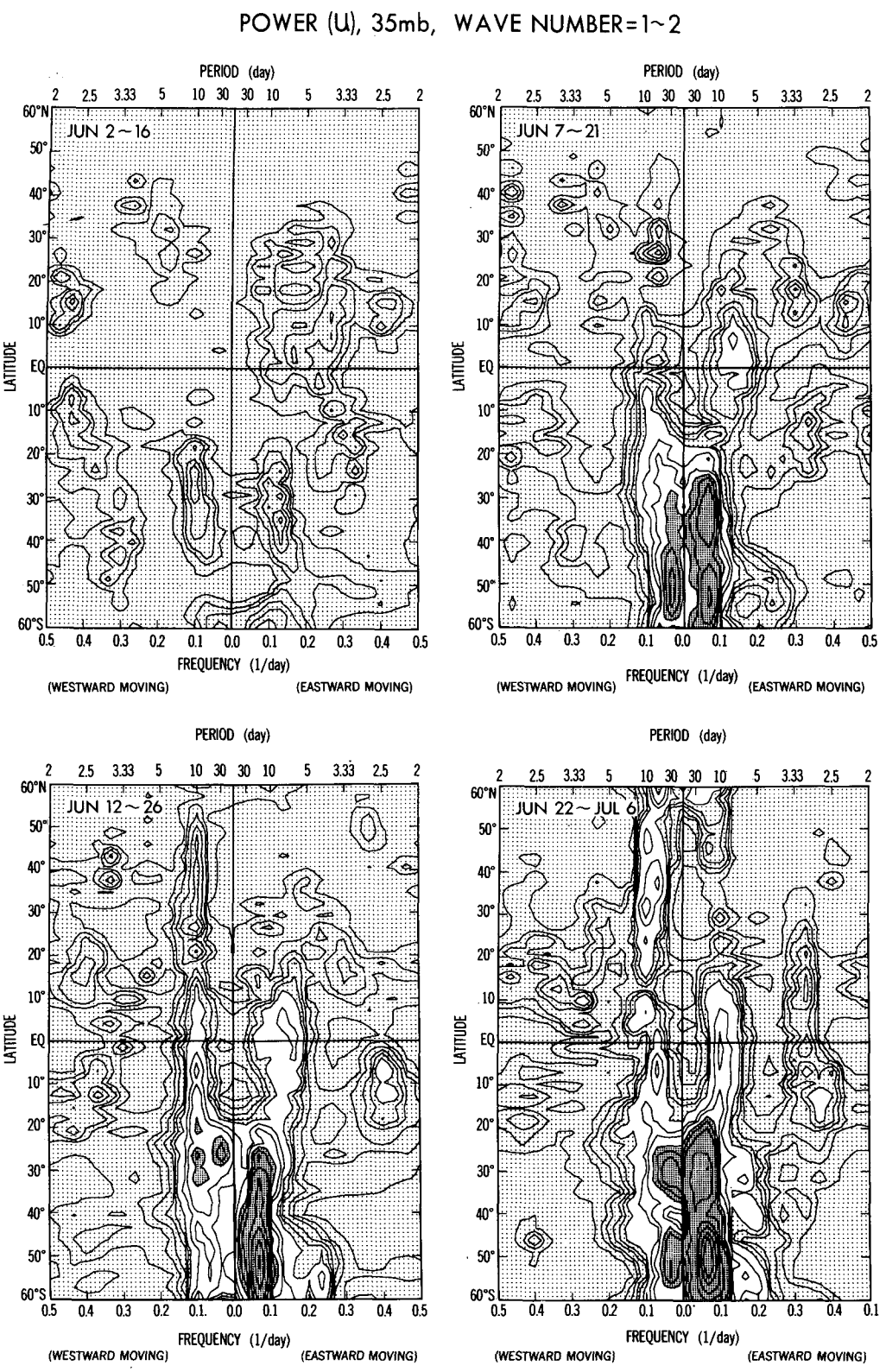

FIG. 5. Frequency-latitude sections of the power spectrum of the zonal wind (wavenumber 1–2) at 35 mb for various time periods. Contour values 1.0, 2.0, 3.0, 5.0, 7.0, 10.0, 20.0, 30.0, 50.0, 70.0, 100.0, 200.0, 300.0, 500.0, 700.0 $m^2 s^{-2}$ day; light shade ≤ 10.0, dark shade ≥ 50.0.

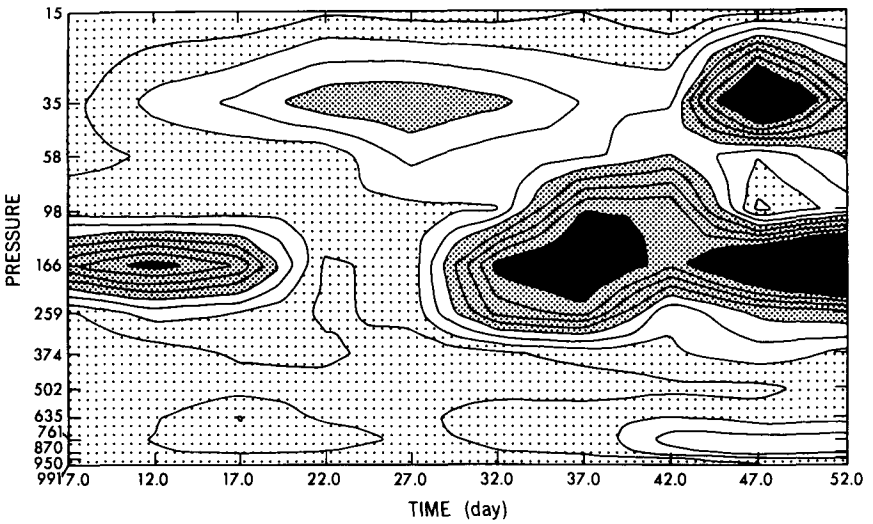

FIG. 6. Time-height section of the power spectrum of the zonal wind (wavenumber 1–2, period 10–15 days, eastward moving) over the equator. Contour interval, 0.25 $m^2 s^{-2}$; light shade, $\leqslant 0.5$, dark shade, $\geqslant 1.0$, black shade, $\geqslant 2.0$.

10–15 days (eastward moving), corresponding to equatorial Kelvin waves. A comparison with the basic model (not illustrated) indicates that the characteristic scale and period of Kelvin waves as well as their amplitude are hardly altered by the elimination of the topographical effects. In Fig. 3a, another peak is seen at wavenumber 1 and 10–20 days period (westward moving) which will be later interpreted as ultralong waves extending from the Southern Hemisphere. In the upper troposphere (Fig. 3b) the power spectrum takes a large value at wavenumber 1–2 and a period of 10–30 days (eastward moving) which may be related to the stratospheric Kelvin wave. Fig. 4 displays the latitude-height distribution of the power spectrum of the eastward moving component of the zonal wind (wavenumber 1–2, period 10–15 days) for 12–26 July. The stratospheric maximum confined over the equator at the 35 mb level corresponds to Kelvin waves. This identification is supported by the fact that the power spectrum of the meridional wind is extremely small (not illustrated). There is also a large value of the power spectrum in the upper tropical troposphere, although it is not isolated from that in midlatitudes.

Next it will be of interest to see how these waves have developed from the small random initial disturbances. Fig. 5 displays four stages of development of eastward moving Kelvin waves and westward moving ultralong waves at 35 mb in the frequency-latitude domain of the power spectrum of the zonal wind (wavenumber 1–2). The top left diagram shows the power spectrum for the first 15-day period (2–16 June). During 7–21 June (top right) eastward moving waves appear over the equator, corresponding to Kelvin waves at their initial stage, while westward moving ultralong waves seem to extend from the Southern Hemisphere toward the equator. For 12–26 June (bottom left), eastward moving Kelvin waves seem to merge with eastward moving ultralong waves appearing in the Southern Hemisphere, while the westward moving wave crosses over the equator. During 22 June–6 July (bottom right) eastward moving Kelvin waves are intensified, while westward moving waves appear also in the Northern Hemisphere.

The temporal development of Kelvin waves is also shown in a time-height section (Fig. 6) of the power spectrum of the zonal wind (wavenumber 1–2, period 10–15 days, eastward moving) over the equator. It seems that waves first grow and then decay in the upper troposphere (166 mb) and are followed by the development of Kelvin waves in the stratosphere (35 mb). This sequence is consistent with the theoretical interpretation by Holton and Lindzen (1968) that stratospheric Kelvin waves are forced from below.

b. The mixed Rossby-gravity wave

A similar analysis has also been made for mixed Rossby-gravity waves appearing in the above experiment. Fig. 7 shows a frequency-wavenumber diagram of the power spectrum of the meridional wind at the 98 mb level over the equator (Fig. 7a) and 40–50°S (Fig. 7b). These figures represent the period 27 June–11 July during which mixed Rossby-gravity waves appear most distinctly in this experiment. Fig. 7a shows a spectral peak at wavenumber 4 and a period of 5 days (westward moving) corresponding to mixed Rossby-gravity waves. A comparison with the basic model (not illustrated) indicates that the charac-

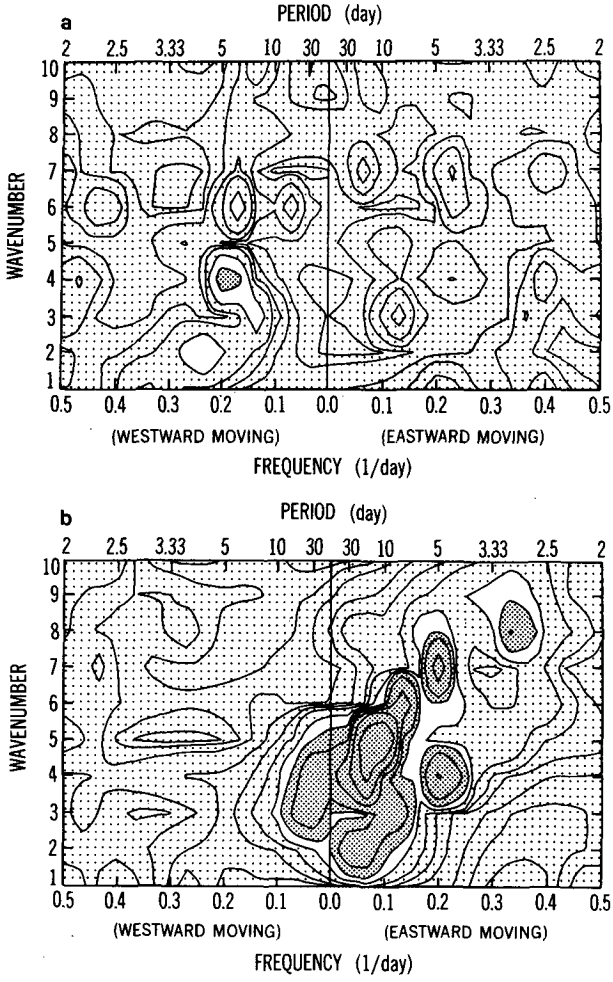

FIG. 7. Frequency-wavenumber diagram of the power spectrum of the meridional wind at 98 mb for the model period 27 June–11 July at the equator (a) and 40–45°S (b). Contour values 0.5, 1.0, 2.0, 5.0, 10.0, 20.0, 50.0, 100.0, 200.0, 500.0 $m^2 s^{-2}$ day; light shade $\leqslant 5.0$, dark shade $\geqslant 10.0$.

teristic scale and period of mixed Rossby-gravity waves as well as their amplitude are hardly altered by elimination of the topographical effects. On the other hand, Fig. 7b is mainly associated with eastward moving components corresponding to cyclone waves (see Hayashi and Golder, 1977, Fig. 4.5). It does not show any spectral peak corresponding to westward moving mixed Rossby-gravity waves with wavenumber 4 and a 5-day period, although there is a large power spectral density at wavenumber 3–5 and periods longer than 15 days. However, this result does not necessarily reject the possibility that the development of mixed Rossby-gravity waves over the equator is somehow related to midlatitude disturbances, as will be discussed later.

Fig. 8 shows the latitude-height distribution of the power spectrum (wavenumber 3–5, period 3.7–6.0 days, westward moving) of the meridional component for the model period 27 June–11 July. The maximum near the tropopause (100 mb) at the equator corresponds to mixed Rossby-gravity waves. This identification is supported by the fact that the power spectrum of the zonal wind attains its minimum over the equator (not illustrated).

Next, we will examine how these mixed Rossby-gravity waves have formed from the initial small random disturbances. Fig. 9 shows four stages of mixed Rossby-gravity waves at 98 mb in frequency-latitude sections of the power spectrum of the meridional wind (wavenumber 3–5).

The top left diagram of Fig. 9 shows that eastward moving waves first appear in the Southern Hemisphere for the first 15 days of integration and can be identified as midlatitude baroclinic waves. During the period 8–22 June (top right), westward moving waves with a 5–6 day period corresponding to mixed Rossby-gravity waves at their initial stage, can be detected over the equator. Concurrently, westward moving waves with a 15-day period branch out from midlatitude disturbances and extend toward the equator. For 12–26 June (bottom left), the westward moving waves with a 15-day period seem to evolve into mixed Rossby-gravity waves with a 5-day period. This shift of period is quantitatively consistent with the Doppler shift by the horizontal shear. It is also consistent with the observational analysis (Zangvil, 1975) of equatorward energy flux of wavenumbers 3–6 whose characteristic period decreases equatorward toward 5 days. For 27 June–11 July (bottom right), mixed Rossby-gravity waves over the equator are fully developed.

The development of mixed Rossby-gravity waves is also shown in a time-height section (Fig. 10) of the power spectrum of the meridional wind (wavenumber 3–5, period 3.7–6.0 days, westward moving) over the equator. It seems that waves appear first in the upper troposphere (250 mb) and are followed by the development of mixed Rossby-gravity waves near the tropopause (100 mb). This sequence is consistent with the theoretical interpretation by Lindzen and Matsuno (1968) that stratospheric mixed Rossby-gravity waves are forced from below.

4. The effect of midlatitude disturbances

Section 3 suggests that midlatitude disturbances may have some influence on the development of equatorial planetary waves. In order to clarify this point, midlatitude disturbances as well as topographical effects are eliminated from the model by setting perturbations to zero poleward of the 30° latitudes at each time step during the course of time integration. It was confirmed by energy integral analysis that there is no leakage of energy from the tropics to extratropical regions due to this cutoff. In order to prevent the zonal mean state from changing drastically in time due to the absence of midlatitude disturbances,

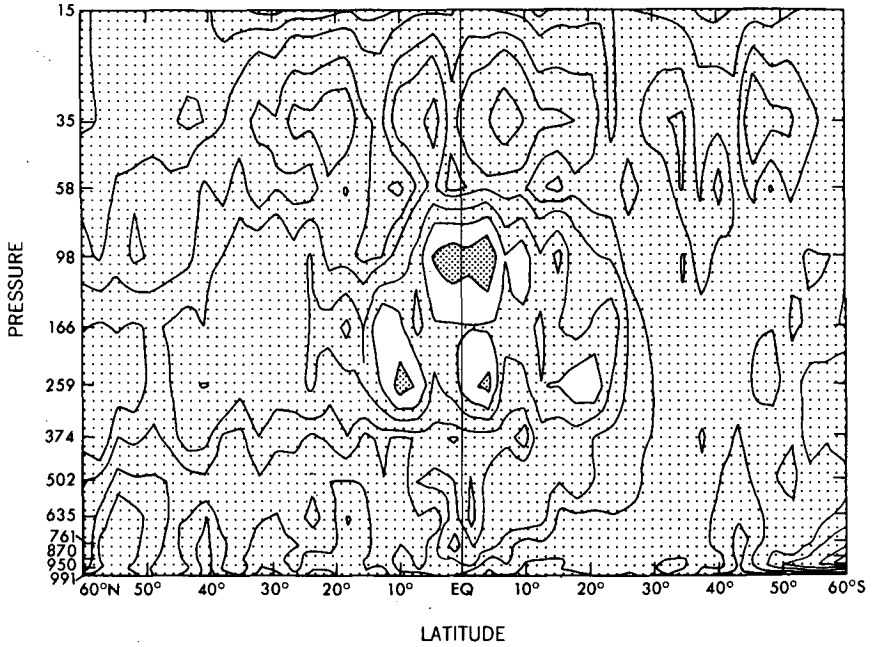

FIG. 8. Latitude-height distribution of the power spectrum of the meridional wind (wavenumber 3–5, period 3.7–6.0 days, westward moving) during the model period June 27–July 11. Contour values 0.1, 0.2, 0.3, 0.5, 0.7, 1.0, 2.0, $m^2 s^{-2}$; light shade $\leqslant 0.7$, dark shade $\geqslant 1.0$.

a fictitious damping proportional to the time-deviation of the zonal means of the predicted variables is incorporated into the model, not only in the midlatitudes, but also in the tropics (see Appendix B for details). For the sake of a fair comparison, the experiment with midlatitude disturbances described in this section has the same damping, since the results are not the same as those without a damping described in the previous section.

Fig. 11 compares experiments with and without midlatitude disturbances. The contours represent the power spectrum of the zonal wind (wavenumber 1–2, period 10–15 days, eastward moving) at the 35 mb level in a latitude-time domain. It is seen that Kelvin waves appear even in the absence of midlatitude disturbances (right-hand part of Fig. 11). This result seems reasonable, since, according to linear theories, Kelvin waves have hardly any meridional wind component to interact with midlatitude disturbances, although some interaction is possible in a nonlinear theory (Murakami, 1974). In contrast to the eastward moving component, the power spectrum of the westward moving component of the zonal wind with wavenumber 1–2 and period 10–15 days was reduced by an order of magnitude (not illustrated) in the stratosphere in the absence of midlatitude disturbances, while it appeared in the troposphere. This supports the interpretation in Section 3 that the westward moving ultralong waves (wavenumber 1–2) in the stratosphere extend from midlatitudes, while those in the troposphere are generated within the tropics.

In contrast to Kelvin waves, it was found that mixed Rossby-gravity waves did not fully develop (less than half in kinetic energy) in the absence of midlatitude disturbances, although they were associated with their characteristic scale and period. This result was confirmed by a further experiment in which midlatitude disturbances are cut off after mixed Rossby-gravity waves are clearly detected over the equator after 20 days of integration. Fig. 12 shows a comparison of the power spectrum of the meridional wind (wavenumber 3–5) with and without midlatitude disturbances. A wide frequency range (period 3.7–15.0 days, westward moving) is chosen so as to include midlatitude waves with periods longer than 5 days. Near the equator, this power spectrum is associated with periods of 4–6 days. It is seen (Fig. 12, right-hand side) that mixed Rossby-gravity waves do not intensify after midlatitude waves are cut off. It should be noted, however, that they do not disappear completely. Their characteristic scale and period was detected, although their amplitude is small. This is because mixed Rossby-gravity waves are generated to some extent by the release of latent heat even in the absence of midlatitude disturbances, as will be confirmed in the next section.

It is also of importance to examine the effect of midlatitude disturbances on the tropical transient eddy kinetic energy as a whole. Fig. 13 compares the total transient eddy kinetic energy (vertical pressure integral) with (left) and without (right) midlatitude disturbances. It should be noted that the total tran-

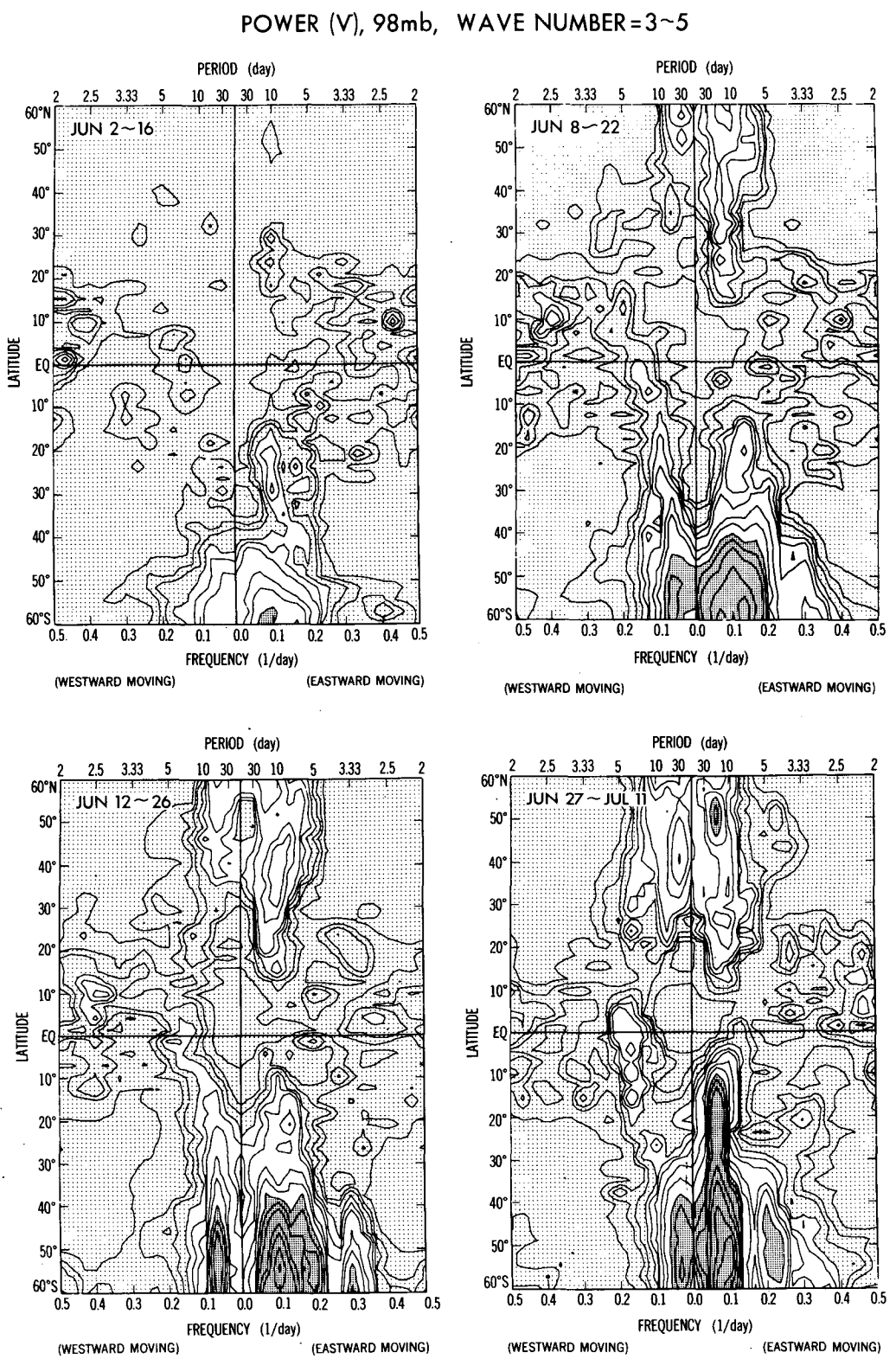

FIG. 9. Frequency-latitude sections of the power spectrum of the meridional wind (wavenumber 3–5) at 98 mb for various time periods. Contour values 1.0, 2.0, 3.0, 5.0, 7.0, 10.0, 20.0, 30.0, 50.0, 70.0, 100.0, 200.0, 300.0, 500.0, 700.0 $m^2 s^{-2}$ day; light shade $\leqslant 5.0$, dark shade $\geqslant 50.0$,

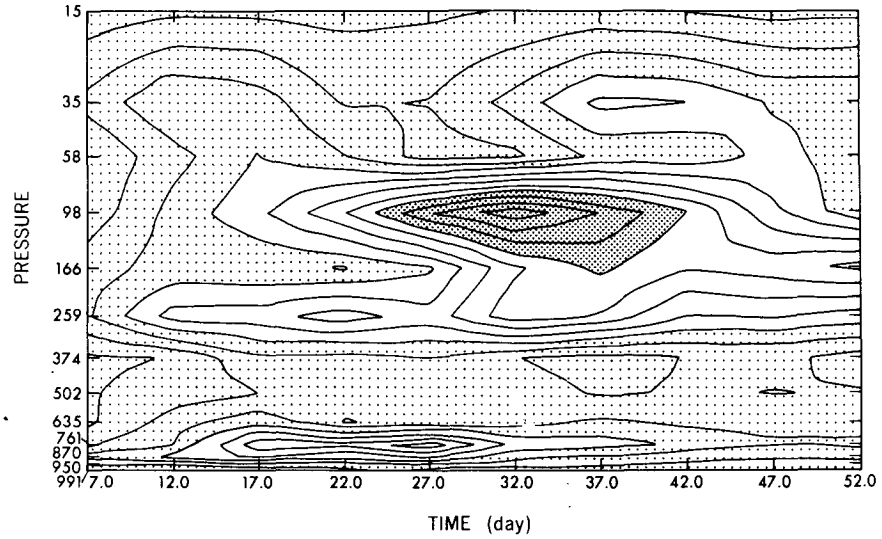

FIG. 10. Time-height section of the power spectrum of the meridional wind (wavenumber 3–5, period 3.7–6.0 days, westward moving) over the equator. Contour interval 0.1 $m^2 s^{-2}$; light shade $\leqslant 0.4$, dark shade $\geqslant 0.8$.

sient eddy kinetic energy (left) does not particularly exhibit a maximum over the equator. This is because stationary waves are absent in this experiment and stratospheric equatorial waves account for only 10% of the vertically integrated transient eddy kinetic energy (see Hayashi, 1974). It is seen (right) that over the equator, the total transient eddy kinetic energy hardly decreases even after midlatitude disturbances are cut off, while in the subtropics it decreases significantly. In contrast to the eddy kinetic energy, the total variance of precipitation (not illustrated) does not decrease even in the subtropics. These results confirm the conclusion by Manabe *et al.* (1974), based on the energetics of their model, that

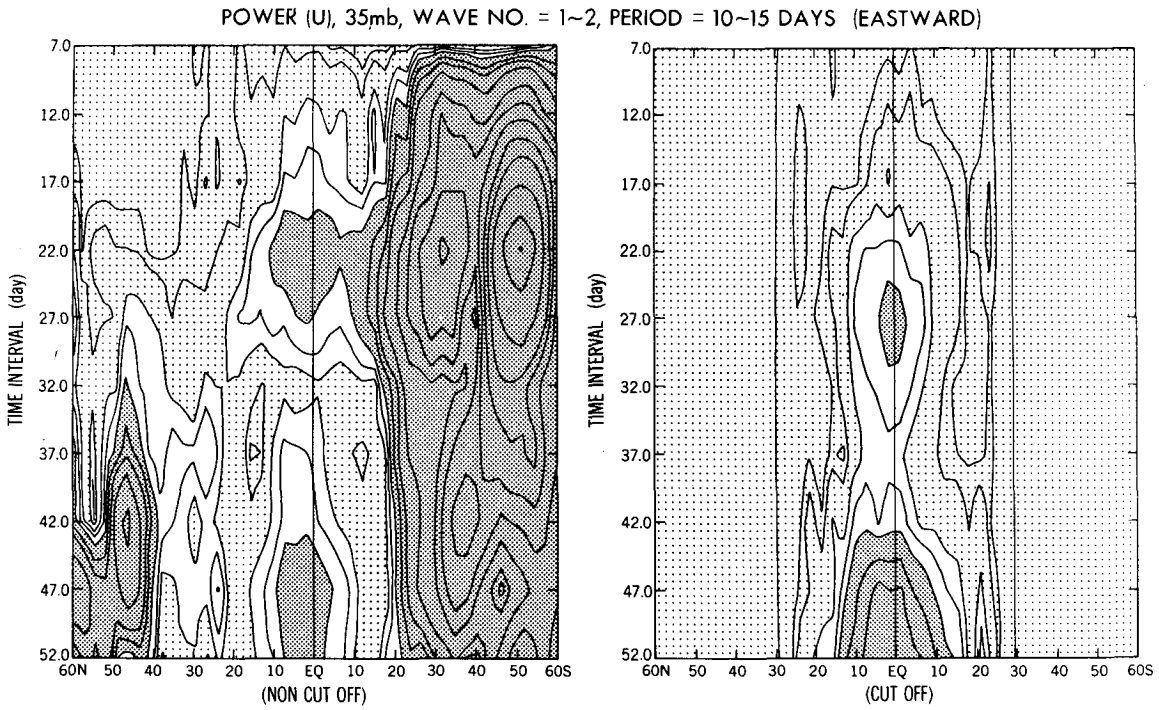

FIG. 11. Latitude-time section of the power spectrum of the zonal wind (wavenumber 1–2, period 10–15 days, eastward moving) at 35 mb with (left) and without (right) midlatitude disturbances. Contour interval 0.25 $m^2 s^{-2}$; light shade $\leqslant 0.5$, dark shade $\geqslant 1.0$.

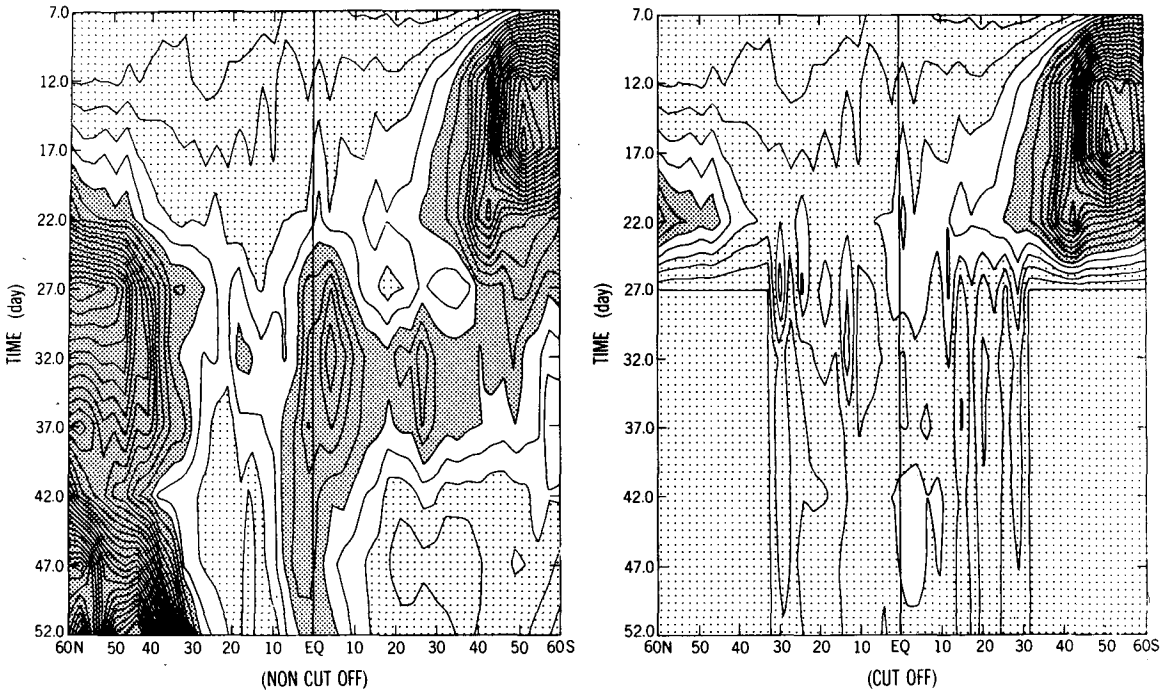

FIG. 12. Latitude-time section of the power spectrum of the meridional wind (wavenumber 3–5, period 3.7–15.0 days, westward moving) at 98 mb. Midlatitude disturbances are cut off after 20 days of time integration (right). Contour interval 0.25 $m^2 s^{-2}$; light shade ≤ 0.75, dark shade ≥ 1.25.

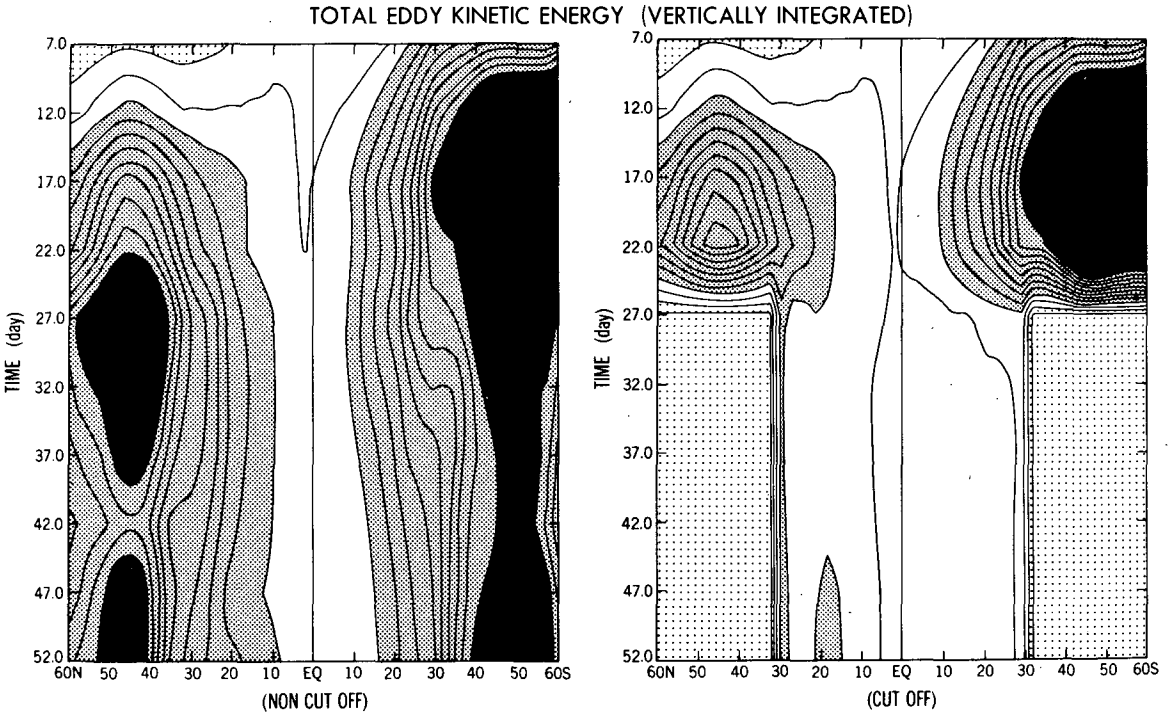

FIG. 13. Latitude-time section of the total transient eddy kinetic energy averaged over 15-day periods and integrated vertically. Midlatitude disturbances are cut off after 20 days of time integration (right). Contour interval 5.0×10^{-3} $m^2 s^{-2}$ mb; light shade ≤ 5.0, dark shade ≥ 15.0, black shade ≥ 95.0.

the total eddy kinetic energy in the equatorial region is maintained primarily by the effect of latent heat release, while in the subtropics the energy flux from midlatitudes is also important.

5. The effect of condensational heat

Section 4 suggests that condensational heat may be responsible for the generation of Kelvin and mixed Rossby-gravity waves, since both these waves appear even in the absence of midlatitude disturbances, although mixed Rossby-gravity waves do not intensify without midlatitude disturbances.

In order to confirm these possibilities, condensational heat as well as midlatitude disturbances were eliminated from the model after 20 days of time integration by eliminating the prognostic system for water vapor. It should be mentioned, however, that by a dry convective adjustment, the vertical temperature gradient is adjusted to the moist adiabatic lapse rate rather than the dry adiabatic lapse rate following Manabe *et al.* (1970). This is because the dry adiabatic lapse rate gives too unrealistic a vertical distribution of temperature. In the dry model, convection can occur in any moist adiabatically unstable layer, whereas in the moist model it is necessary for the air to be saturated in order for condensation and moist convection to take place.

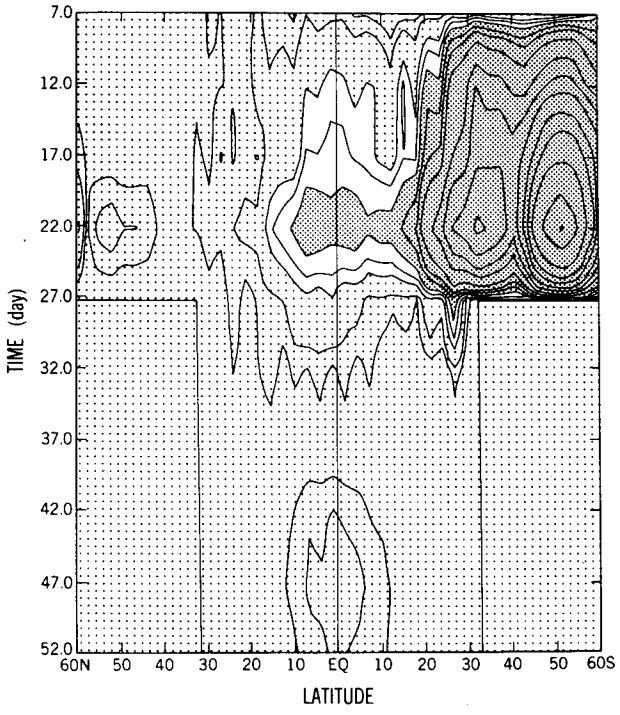

FIG. 14. Latitude-time section of the power spectrum of the zonal wind (wavenumber 1–2, period 10–15 days, eastward moving) at 35 mb. Both midlatitude disturbances and latent heat release have been cut off after 20 days of time integration. Contour interval 0.25 $m^2 s^{-2}$; light shade $\leqslant 0.5$, dark shade $\geqslant 1.0$.

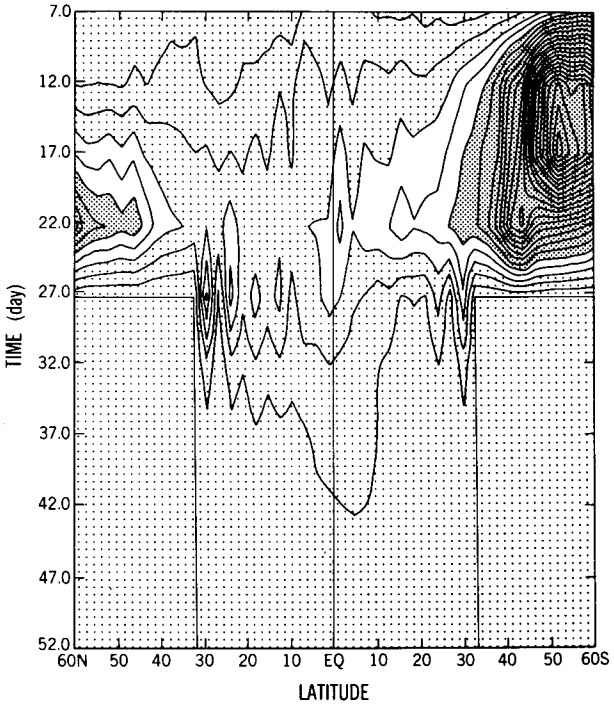

FIG. 15. Latitude-time section of the power spectrum of the meridional wind (wavenumber 3–5, period 3.7–15.0 days, westward moving) at 98 mb. Both midlatitude disturbances and latent heat release are cut off after 20 days of time integration. Contour interval 0.25 $m^2 s^{-2}$; light shade $\leqslant 0.75$, dark shade $\geqslant 1.25$.

Fig. 14 shows that the power spectrum (wavenumber 1–2, period 10–15 days, eastward moving) of the zonal wind at the 35 mb level corresponding to Kelvin waves diminishes drastically after the cutoff. This means that Kelvin waves are generated primarily due to the effect of condensational heating. Fig. 15 shows that the power spectrum of the meridional wind at 98 mb corresponding to mixed Rossby-gravity waves disappears completely after the cutoff. This result was confirmed by eliminating only condensational heating, while midlatitude disturbances are retained. These results are interpreted to mean that mixed Rossby-gravity waves are generated to some extent due to the effect of condensational heat and are enhanced significantly by midlatitude disturbances. Similarly, Fig. 16 shows that the total transient eddy kinetic energy diminishes drastically after the cutoff. This means that the total transient eddy kinetic energy over the equator is generated primarily due to the effect of condensational heating as demonstrated by Manabe *et al.* (1970) by comparing dry and moist models.

6. Conclusions and remarks

By eliminating the effects of topography, midlatitude disturbances and condensational heat successively

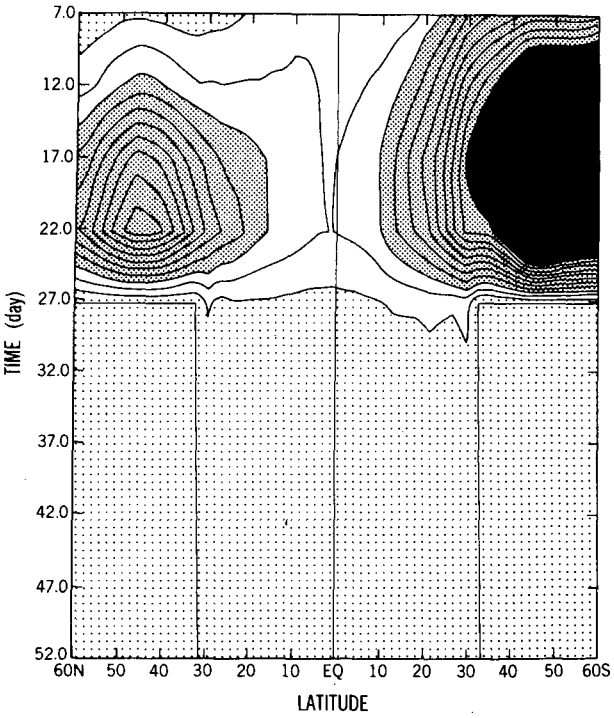

FIG. 16. Latitude-time section of the power spectrum of the total transient eddy kinetic energy averaged over 15-day periods and integrated vertically. Both midlatitude disturbances and latent heat release are cut off after 20 days of integration. Contour interval 5.0×10^{-3} m^2 s^{-2} mb; light shade $\leqslant 5.0$, dark shade $\geqslant 15.0$, black shade $\geqslant 95.0$.

from a general circulation model, the following results were obtained:

1) The amplitude and the characteristic scale and period of both Kelvin and mixed Rossby-gravity waves are hardly affected by the land-sea contrast or the zonal variation of sea surface temperature.

2) Kelvin waves are hardly affected by midlatitude disturbances, but diminish drastically after condensational heat is also eliminated.

3) Mixed Rossby-gravity waves are significantly reduced in amplitude by the elimination of midlatitude disturbances. They diminish completely after latent heat is also eliminated.

4) The total kinetic energy of all equatorial transient disturbances is generated primarily as the result of latent heat release in the tropics, while that of subtropical transient disturbances is reduced significantly in the absence of midlatitude disturbances.

It is of interest to compare the above results with the existing theories. The present results are consistent with these theories in that the topographical effect is not an essential factor for the characteristic scale and period of both Kelvin and mixed Rossby-gravity waves. The present results are similar to those of both the CISK and random thermal forcing theories in that both Kelvin and mixed Rossby-gravity waves appear in the stratosphere as a result of latent heat release in the troposphere. On the other hand, the present results are also similar to those of the lateral forcing theories in that mixed Rossby-gravity waves can be significantly enhanced by midlatitude disturbances. However, these waves are not generated by midlatitude disturbances in the absence of condensational heat as confirmed by eliminating only condensational heating.

Although the above theories have their own drawbacks as described in the Introduction, they should not be entirely rejected since a nonlinear effect is neglected. It is of importance to improve on these theories in order to interpret the results of the present experiments theoretically.

Acknowledgments. The authors wish to express their hearty appreciation to Dr. S. Manabe whose initial guidance, valuable suggestions and comments were indispensable for the present work. We are also grateful to Drs. K. Miyakoda and I. Orlanski for their critical review, and Dr. J. Smagorinsky for his interest and encouragement. We are indebted to the members of the GFDL staff, who contributed to the construction of the efficient models used in this experiment, especially D. Daniel and M. Spelman. We are also indebted to those who assisted in the preparation of the manuscript, P. Tunison for drafting, J. Conner for photography and E. Thompson for typing.

APPENDIX A

Space-time Spectral Formulas

The space-time power spectrum $P_{\kappa,\pm\omega}$ of space-time series $W(x,t)$ can be computed by the following formulas:

Real representation (Hayashi, 1971b):

$$4P_{\kappa,\pm\omega}(W)=P_\omega(C_\kappa)+P_\omega(S_\kappa)\pm 2Q_\omega(C_\kappa,S_\kappa) \quad \text{(A1)}$$

Complex representation (Hayashi, 1977):

$$4P_{\kappa,\pm\omega}(W)=P_{\pm\omega}(C_\kappa-iS_\kappa), \text{ where } i^2=-1. \quad \text{(A2)}$$

The positive and negative frequencies $\pm\omega$ indicate retrogressive and progressive waves, respectively. In the above C_κ and S_κ are space cosine and sine coefficients with wavenumber κ and P_ω, Q_ω are time-power and quadrature spectra, respectively, with frequency ω.

The real representation (A1) is convenient for applying the conventional lag method or direct Fourier transform method. On the other hand, the complex representation (A2) is suitable for applying the recent maximum entropy method. [See Ulrych and Bishop (1975) for a review and Hayashi (1977) for its application to space-time spectral analysis.]

APPENDIX B

A Numerical Scheme for Restoring the Zonal Mean to its Initial Value

In order to prevent the zonal mean state from changing drastically in time, a fictitious damping proportional to the deviation of the zonal mean of the prognostic variables $\bar{T}(t)$ from its initial value $\bar{T}(0)$ is incorporated as

$$\frac{\partial T(t)}{\partial t}=F(t)-\gamma[\bar{T}(t)-\bar{T}(0)], \tag{B1}$$

where F is the forcing term, γ the damping coefficient and the overbar denotes the zonal mean.

In the following, we shall introduce a convenient numerical scheme (B4) by which the damping term can be incorporated as a correction to $T^*(\tau+1)$ which is predicted by a model without the damping.

First, $T^*(\tau+1)$ is predicted in the absence of the damping as

$$T^*(\tau+1)=T(\tau-1)+2\Delta tF(\tau). \tag{B2}$$

Then $T(\tau+1)$ is predicted in principle by (B1) as

$$T(\tau+1)=T(\tau-1)+2\Delta tF(\tau) -2\gamma\Delta t[\bar{T}^*(\tau+1)-\bar{T}(0)]. \tag{B3}$$

Eliminating $F(\tau)$ between (B.2) and (B.3), we have

$$T(\tau+1)=T^*(\tau+1)-\bar{T}^*(\tau+1) +[(1-2\gamma\Delta t)\bar{T}^*(\tau+1)+2\gamma\Delta t\bar{T}(0)]. \tag{B4}$$

This means that the effect of the damping is to replace the predicted zonal mean $\bar{T}^*(\tau+1)$ by a weighted mean of $\bar{T}^*(\tau+1)$ and the initial zonal mean $\bar{T}(0)$.

The damping time can be estimated by (B6) as follows. Taking a zonal mean of (B2) and (B3) and eliminating $\bar{T}^*(\tau+1)$ between them, we have

$$\bar{T}(\tau+1)-\bar{T}(0)=(1-2\gamma\Delta t)[\bar{T}(\tau-1)-\bar{T}(0)] +(1-2\gamma\Delta t)\bar{F}(\tau)2\Delta t. \tag{B5}$$

If the forcing $F(\tau)$ is omitted, (B5) gives

$$\frac{\bar{T}(\tau+1)-\bar{T}(0)}{\bar{T}(1)-\bar{T}(0)}=(1-2\gamma\Delta t)^{\tau/2}. \tag{B6}$$

In the present experiment, the value of γ is chosen in such a way that

$$\left.\begin{aligned}\Delta t=240\text{ s},\quad \tau\Delta t=1\text{ day}\\ (1-2\gamma\Delta t)^{\tau/2}=0.1\end{aligned}\right\}. \tag{B7}$$

This means that according to (B6), the time deviation of the zonal mean is reduced to 10% of its value at $\tau=1$ by the damping after 1 day of time integration.

REFERENCES

Andrews, D. G., and M. E. McIntyre, 1976: Planetary waves in horizontal and vertical shear: The generalized Eliassen–Palm relation and the mean zonal acceleration. *J. Atmos. Sci.*, **33**, 2031–2048.

Arakawa, A., and W. H. Schubert, 1974: Interaction of a cumulus cloud ensemble with the large-scale environment. Part I. *J. Atmos. Sci.*, **31**, 674–701.

Bennet, J. R., and J. A. Young, 1971: The influence of latitudinal wind shear upon large-scale wave propagation into the tropics. *Mon. Wea. Rev.*, **99**, 202–214.

Chang, C. P., 1974: A note on the laterally forced wave motions in the tropics. *J. Meteor. Soc. Japan*, **52**, 247–249.

——, 1976a: Vertical structure of tropical waves maintained by internally-induced cumulus heating. *J. Atmos. Sci.*, **33**, 729–739.

——, 1976b: Forcing of stratospheric Kelvin waves by tropospheric heat sources. *J. Atmos. Sci.*, **33**, 740–744.

Charney, J. G., 1969: A further note on large-scale motions in the tropics. *J. Atmos. Sci.*, **26**, 182–185.

Dickinson, R. E., 1968: Planetary Rossby waves propagating vertically through weak wind wave guides. *J. Atmos. Sci.*, **25**, 984–1002.

Gambo, K., 1971: A note on the Rossby and gravity waves on a rotating sphere. *J. Meteor. Soc. Japan*, **49** (Special Issue), 678–690.

Hayashi, Y., 1970: A theory of large-scale equatorial waves generated by condensation heat and accelerating the zonal wind. *J. Meteor. Soc. Japan*, **48**, 140–160.

——, 1971a: Instability of large-scale equatorial waves with a frequency-dependent CISK parameter. *J. Meteor. Soc. Japan*, **49**, 59–62.

——, 1971b: A generalized method of resolving disturbances into progressive and retrogressive waves by space-Fourier and time-cross spectral analyses. *J. Meteor. Soc. Japan*, **49**, 125–128.

——, 1974: Spectral analysis of tropical disturbances appearing in a GFDL general circulation model. *J. Atmos. Sci.*, **31**, 180–218.

——, 1976: Non-singular resonance of equatorial waves under the radiation condition. *J. Atmos. Sci.*, **33**, 183–201.

——, 1977: Space-time power spectral analysis using the maximum entropy method. *J. Meteor. Soc. Japan*, **55**, 415–420.

——, and D. G. Golder, 1977: Space-time spectral analysis of mid-latitude disturbances appearing in a GFDL general circulation model. *J. Atmos. Sci.*, **34**, 237–262.

Holloway, J. L., Jr., M. J. Spelman and S. Manabe, 1973: Latitude-longitude grid suitable for numerical time integration of a global atmospheric model. *Mon. Wea. Rev.*, **101**, 69–78.

Holton, J. R., 1972: Waves in the equatorial stratosphere generated by tropospheric heat sources. *J. Atmos. Sci.*, **29**, 368–375.

——, 1973: On the frequency distribution of atmospheric Kelvin waves. *J. Atmos. Sci.*, **30**, 499–501.

——, and R. S. Lindzen, 1968: A note on Kelvin waves in the atmosphere. *Mon. Wea. Rev.*, **96**, 385–386.

Itoh, H., 1977: The response of equatorial waves to thermal forcing. *J. Meteor. Soc. Japan*, **55**, 222–239.

——, 1978: Forced equatorial waves under the marginally stable state with respect to wave-CISK mechanism. *J. Meteor. Soc. Japan*, **56**, 145–158.

Kuo, H. K., 1975: Instability theory of large-scale disturbances in the tropics. *J. Atmos. Sci.*, **32**, 2229–2245.

Lamb, V. R., 1973: The response of a tropical atmosphere to middle latitude forcing. Ph.D. thesis. University of California, Los Angeles, 151 pp.

Lindzen, R. S., 1967: Planetary waves on beta planes. *Mon. Wea. Rev.*, **95**, 441–451.

——, 1970: Vertical momentum transport by large-scale disturbances of the equatorial stratosphere. *J. Meteor. Soc. Japan*, **48**, 81–82.

——, 1974: Wave-CISK in the tropics. *J. Atmos. Sci.*, **31**, 156–179.

——, and T. Matsuno, 1968: On the nature of large-scale wave disturbances in the equatorial lower stratosphere. *J. Meteor. Soc. Japan*, **46**, 215–221.

Mak, M. K., 1969: Laterally driver stochastic motions in the tropics. *J. Atmos. Sci.*, **26**, 41–64.

Manabe, S., J. L. Holloway, Jr., and H. M. Stone, 1970: Tropical circulation in a time integration of a global model of the atmosphere. *J. Atmos. Sci.*, **27**, 580–613.

——, D. G. Hahn and J. L. Holloway, Jr., 1974: The seasonal variation of the tropical circulation as simulated by a global model of the atmosphere. *J. Atmos. Sci.*, **31**, 43–83.

——, K., Bryan and M. J. Spelman, 1975: A global ocean-atmosphere climate model. Part I. The atmospheric circulation. *J. Phys. Oceanogr.*, **5**, 3–29.

Matsuno, T., 1966: Quasi-geostrophic motions in the equatorial area. *J. Meteor. Soc. Japan*, **44**, 25–43.

Murakami, M., 1973: Response of the tropical atmosphere to the initial forcing on the equator and the middle latitude boundary. *J. Meteor. Soc. Japan*, **51**, 252–262.

——, 1974: Influence of mid-latitudinal planetary waves on the tropics under the existence of critical latitude. *J. Meteor. Soc. Japan*, **52**, 261–272.

Reed, R. J., W. J. Campbell, L. A. Rasmussen and D. G. Rogers, 1961: Evidence of a downward-propagating annual wind reversal in the equatorial stratosphere. *J. Geophys. Res.*, **66**, 813–818.

Rosenthal, S. L., 1965: Some preliminary theoretical considerations of tropospheric wave motions in equatorial latitudes. *Mon. Wea. Rev.*, **93**, 605–612.

Stark, T. E., 1976: Wave-CISK and cumulus parameterization. *J. Atmos. Sci.*, **33**, 2383–2391.

Tsay, C. Y., 1974: Analysis of large-scale wave disturbances in the tropics simulated by an NCAR global circulation model. *J. Atmos. Sci.*, **31**, 330–339.

Ulrych, T. J., and T. N. Bishop, 1975: Maximum entropy spectral analysis and autoregressive decomposition. *Rev. Geophys. Space Phys.*, **13**, 183–200.

Wallace, J. M., and V. E. Kousky, 1968: Observational evidence of Kelvin waves in the tropical stratosphere. *J. Atmos. Sci.*, **25**, 900–907.

Yamasaki, M., 1969: Large-scale disturbances in a conditionally unstable atmosphere in low latitudes. *Pap. Meteor. Geophys.*, **20**, 289–336.

Yanai, M., and T. Maruyama, 1966: Stratospheric wave disturbances propagating over the equatorial Pacific. *J. Meteor. Soc. Japan*, **44**, 291–294.

Zangvil, A., 1975: Upper tropospheric waves in the tropics and their association with clouds in the wavenumber-frequency domain. Ph.D. thesis, Meteor. Pap. Nos. 13 and 14, University of California, Los Angeles, 131 pp.